NEK2 knockdown enhances oxaliplatin responsiveness by weakening HIF-1α/SLC7A11-dependent GSH/GPX4 antioxidant defense against ferroptosis in gastric cancer cells

LAIZHEN TOU[1], HUA SHI[2], HONGTAO XU[1], CHUAN JIANG[1], DAN WU[1], ZHENG SUN[1], JUNHAO LI[1], KANG YANG[1] and JINGJING ZHENG[1]

[1]Gastrointestinal Surgery, Lishui Municipal Central Hospital, The Fifth Affiliated Hospital of Wenzhou Medical University, Lishui, Zhejiang 323000, P.R. China; [2]Department of Gastroenterology, Lishui Municipal Central Hospital, The Fifth Affiliated Hospital of Wenzhou Medical University, Lishui, Zhejiang 323000, P.R. China

Received June 30, 2026; Accepted November 10, 2026

DOI: 10.3892/or.2026.9228

Abstract. Oxaliplatin (OXA) is widely used in chemotherapy for advanced gastric cancer (GC), yet treatment responses are often suboptimal. Despite the established role of NIMA-related kinase 2 (NEK2) in promoting GC progression, its contribution to OXA responsiveness and the underlying molecular mechanisms remain poorly understood. AGS and HGC-27 GC cells were subjected to small interfering RNA-mediated NEK2 knockdown and OXA treatment. Cell viability, proliferation and apoptosis were evaluated by Cell Counting Kit-8, 5-ethynyl-2'-deoxyuridine incorporation and flow cytometry, respectively. Gene expression and transcriptional regulation were examined using reverse transcription-quantitative PCR, western blotting, chromatin immunoprecipitation-quantitative PCR and luciferase reporter assays, together with overexpression-based rescue experiment. Antioxidant defense and ferroptosis-related oxidative damage were assessed using biochemical and flow cytometric assays, with ferroptosis inducers and inhibitors used for functional validation. NEK2 knockdown enhanced OXA-induced growth inhibition and apoptosis in AGS and HGC-27 cells. Mechanistically, NEK2 promoted hypoxia-inducible factor-1α (HIF-1α)/solute carrier family 7 member 11 (SLC7A11) signaling through β-catenin activation, while HIF-1α overexpression partially attenuated the enhanced OXA responsiveness induced by NEK2 knockdown. Further investigation revealed that NEK2 knockdown compromised HIF-1α/SLC7A11-dependent glutathione (GSH)/glutathione peroxidase 4 (GPX4) antioxidant defense, thereby increasing cellular susceptibility to ferroptosis and exacerbating OXA-induced ferroptosis-related oxidative damage, as evidenced by increased reactive oxygen species, malondialdehyde accumulation and lipid peroxidation. Moreover, treatment with the ferroptosis inhibitors ferrostatin-1 or liproxstatin-1 partially attenuated the enhanced OXA responsiveness associated with NEK2 knockdown, further supporting the involvement of ferroptosis in this process. Collectively, these findings suggest that NEK2 knockdown enhances OXA responsiveness by disrupting HIF-1α/SLC7A11-dependent GSH/GPX4 antioxidant defense and promoting ferroptosis in GC cells. Targeting NEK2 may therefore represent a potential strategy for improving OXA responsiveness in GC.

Introduction

Gastric cancer (GC) remains a major global health burden, ranking fifth worldwide in both incidence and cancer-related mortality (1). The non-specific symptoms associated with early-stage GC often hinder timely diagnosis, resulting in numerous patients presenting with advanced-stage disease (2). Oxaliplatin (OXA)-based chemotherapy is widely used in the treatment of advanced GC (3); however, insufficient treatment responses frequently limit its clinical efficacy (4,5). Therefore, elucidating the molecular determinants of OXA responsiveness is essential for identifying novel strategies to enhance its antitumor efficacy and improve treatment outcomes.

NIMA-related kinase 2 (NEK2) is a centrosome-associated serine/threonine kinase that plays a crucial role in cell division and mitotic regulation. Its aberrant expression has been implicated in tumor progression and resistance to anticancer therapies (6), highlighting NEK2 as a potential therapeutic target (7). Notably, a comparative *in vitro* screen across 19 cancer cell lines identified GC cells as particularly sensitive to the NEK2 inhibitor MBM-5 (8), suggesting that NEK2 may have functional relevance in GC biology. Consistent with these findings, NEK2 has been shown to promote GC cell proliferation and tumor growth through multiple oncogenic

Correspondence to: Professor Jingjing Zheng, Gastrointestinal Surgery, Lishui Municipal Central Hospital, The Fifth Affiliated Hospital of Wenzhou Medical University, 289 Kuocang Road, Lishui, Zhejiang 323000, P.R. China
E-mail: zhengjj008@126.com

Key words: NIMA-related kinase 2, hypoxia-inducible factor-1α, solute carrier family 7 member 11, glutathione, glutathione peroxidase 4, oxaliplatin, gastric cancer

signaling and epigenetic regulatory mechanisms, including AKT/hypoxia-inducible factor-1α (HIF-1α), ERK/MAPK and β-catenin-associated signaling (9-11). Beyond its role in tumor progression, NEK2 has been implicated in resistance to several anticancer agents in other malignancies (12-14), suggesting that it may contribute to the regulation of chemotherapy responsiveness. However, whether NEK2 influences OXA responsiveness in GC and the molecular mechanisms underlying this potential effect remain unclear.

Ferroptosis is an iron-dependent form of regulated cell death characterized by excessive lipid peroxidation and is distinct from apoptosis, necrosis and pyroptosis (15). Accumulating evidence suggests that suppression of ferroptosis contributes to OXA resistance in GC, whereas promoting ferroptosis can enhance the antitumor effects of OXA (16,17). Notably, a previous study by the authors demonstrated that NEK2 knockdown increases ferroptosis susceptibility in GC cells through Keap1/Nrf2/HMOX1 signaling (18), raising the possibility that ferroptosis also contributes to NEK2-mediated regulation of OXA responsiveness.

A key cellular defense against ferroptosis is the glutathione (GSH)/glutathione peroxidase 4 (GPX4) antioxidant system, which limits the accumulation of lipid peroxides (19). This protective system relies on solute carrier family 7 member 11 (SLC7A11)-mediated cystine uptake to support GSH synthesis and maintain GPX4-dependent detoxification of lipid peroxides (20), thereby contributing to OXA resistance (21). HIF-1α has been shown to directly activate SLC7A11 transcription by binding to its promoter and enhancing its transcriptional activity (22,23). In addition, HIF-1α has also been implicated in oncogenic signaling associated with OXA resistance and poor prognosis in several cancers (24). Given that NEK2 has been reported to upregulate HIF-1α expression (9), NEK2 may promote OXA resistance by sustaining HIF-1α/SLC7A11 signaling and downstream GSH/GPX4-dependent antioxidant defense. However, whether this mechanism contributes to NEK2-mediated OXA responsiveness in GC remains unclear.

In the present study, it was investigated whether NEK2 knockdown enhances OXA-induced growth inhibition and cell death in GC cells. The underlying mechanism was further explored by examining the regulatory relationship between NEK2 and HIF-1α/SLC7A11 signaling and it was investigated whether HIF-1α restoration attenuates the effect of NEK2 knockdown in OXA responsiveness. In addition, it was assessed whether NEK2 knockdown impairs HIF-1α/SLC7A11-dependent GSH/GPX4 antioxidant defense, thereby increasing ferroptosis susceptibility and exacerbating OXA-induced ferroptosis-related oxidative damage. Finally, ferroptosis inhibitors were employed to clarify the functional contribution of ferroptosis to the enhanced OXA responsiveness following NEK2 knockdown.

Materials and methods

Cell culture. Human gastric adenocarcinoma AGS and HGC-27 cells were obtained from the Cell Bank of the Chinese Academy of Sciences (cat. no. SCSP-5262) and Procell Life Science & Technology Co., Ltd. (cat. no. CL-0107), respectively. AGS cells were cultured in Ham's F-12K medium (cat. no. 21127022; Gibco; Thermo fisher Scientific, Inc.) supplemented with 10% fetal bovine serum (FBS; cat. no. A5670701; Gibco; Thermo fisher Scientific, Inc.), and HGC-27 cells were cultured in RPMI-1640 medium (cat. no. PM150110; Procell Life Science & Technology Co., Ltd.) supplemented with 10% FBS. Both cell lines were maintained at 37˚C in an incubator with 5% CO_2 and passaged at a ratio of 1:3.

Cell treatment. OXA (cat. no. HY-17371), RSL3 (cat. no. HY-100218A), FIN56 (cat. no. HY-103087), ferrostatin-1 (Fer-1; cat. no. HY-100579) and liproxstatin-1 (cat. no. HY-12726) were purchased from MedChemExpress. OXA was dissolved in sterile water to prepare a 5 mM stock solution, whereas RSL3, FIN56, Fer-1 and liproxstatin-1 were dissolved in dimethyl sulfoxide to prepare 10 mM stock solutions. All stock solutions were aliquoted and stored at -80˚C, with OXA and Fer-1 protected from light, to avoid repeated freeze-thaw cycles. Working solutions were freshly prepared by dilution in culture medium before use.

GC cells were treated with OXA (0, 0.5, 2, 8, 32, and 128 μM) for 24 h. For ferroptosis-related experiments, AGS cells were treated with RSL3 (2 μM) or FIN56 (5 μM) for 12 h, or with Fer-1 (2 μM) or liproxstatin-1 (1 μM) for 24 h. Following treatment, cells were collected for subsequent analyses.

Cell viability assay. GC cells were seeded into 96-well plates at $3x10^3$ cells/well and exposed to different concentrations of OXA for 24 h. Cell viability was then assessed using the Cell Counting Kit-8 (CCK-8) assay. Briefly, CCK-8 reagent (cat. no. C0038; Beyotime Institute of Biotechnology) was added to each well at a final concentration of 10%, and cells were incubated at 37˚C for 30 min. Absorbance at 450 nm was measured using a SpectraMax M3 microplate reader (Molecular Devices, LLC).

Cell transfection. GC cells were transfected when they reached ~70% confluence. Before transfection, the culture medium was replaced with serum-free Opti-MEM medium (cat. no. 31985; Gibco; Thermo Fisher Scientific, Inc.). For plasmid transfection, 3 μg of HIF-1α overexpression plasmid (VB261107-1056znq; VectorBuilder) or β-catenin overexpression plasmid (VB900033-0063cgz; VectorBuilder) was diluted in 250 μl Opti-MEM. For small interfering RNA (siRNA) transfection, NEK2-targeting siRNA (Shanghai GenePharma Co., Ltd.) was diluted in 250 μl Opti-MEM to a final concentration of 20 nM. The siRNA sequences were as follows: si-negative control (siNC) sense, 5'-UUCUCC GAACGUGUCACGUTT-3' and antisense, 5'-ACGUGA CACGUUCGGAGAATT-3'; siNEK2#1 sense, 5'-GGCACA CCUUAUUACAUGUTT-3' and antisense, 5'-ACAUGUAAU AAGGUGUGCCTT-3'; siNEK2#2 sense, 5'-GAUCUGGCU AGUGUAAUUATT-3' and antisense, 5'-UAAUUACAC UAGCCAGAUCTT-3'. Lipofectamine™ 2000 reagent (6 μl; cat. no. 11668-019; Invitrogen; Thermo Fisher Scientific, Inc.) was diluted separately in 250 μl Opti-MEM. After incubation for 5 min, the diluted nucleic acids and Lipofectamine™ 2000 were combined and incubated for 20 min at room temperature. The mixture was then added to the cells and incubated for 6 h, after which the medium was replaced with complete culture medium. Cells were harvested or used for subsequent experiments 72 h after transfection.

Reverse transcription-quantitative PCR (RT-qPCR). Total RNA was extracted using TRI Reagent (cat. no. T9424; MilliporeSigma), and RNA concentration was determined using a NanoDrop 2000c spectrophotometer (Thermo Fisher Scientific, Inc.). Total RNA was reverse transcribed using Master Mix (cat. no. RR036A; Takara Bio, Inc.). qPCR was performed using the TB-Green qPCR kit (cat. no. RR420A; Takara) on an Applied Biosystems 7300 Real-time PCR system (Thermo Fisher Scientific, Inc.). The thermal cycling conditions were as follows: Initial denaturation at 95˚C for 30 sec, followed by 40 cycles of denaturation at 95˚C for 5 sec and annealing/extension at 60˚C for 31 sec. Relative mRNA expression was calculated using the $2^{-\Delta\Delta Cq}$ method (25,26) after normalization to GAPDH. The primer sequences were as follows: NEK2 forward, 5'-CTGTCTCTGGCAAGTAATCCAG-3' and reverse, 5'-CAGGTCCTTGCACTTGGACT-3'; HIF-1α forward, 5'-GTACCCTAACTAGCCGAGGAAGAA-3' and reverse, 5'-GTGAATGTGGCCTGTGCAGT-3'; SLC7A11 forward, 5'-TGGAACGAGGAGGTGGAGAA-3' and reverse, 5'-TGTGCTTTTTCCTTCACAGCG-3'; β-catenin forward, 5'-CACAAGCAGAGTGCTGAAGGTG-3' and reverse, 5'-GATTCCTGAGAGTCCAAAGACAG-3'; and GAPDH forward, 5'-GAAGGTGAAGGTCGGAGTC-3' and reverse, 5'-GAAGATGGTGATGGGATTTC-3'.

5-ethynyl-2'-deoxyuridine (EdU) incorporation assay. Cell proliferation was evaluated using the BeyoClick™ EdU-555 kit (cat . no. C0075S; Beyotime Institute of Biotechnology) according to the manufacturer's instructions. Briefly, cells cultured in 12-well plates were incubated with EdU working solution for 3 h. The cells were then washed with PBS, fixed with 4% paraformaldehyde for 30 min, and permeabilized with 0.3% Triton X-100 in PBS. Incorporated EdU was subjected to click-chemistry detection. After washing with PBS, cell nuclei were counterstained with DAPI (1 μg/ml; cat. no. C1006; Beyotime Institute of Biotechnology) for 5 min. The cells were subsequently washed with PBS, and images were captured and analyzed using a fluorescence microscope (BX53; Olympus Corporation).

Annexin V-FITC/7-AAD apoptosis assay. Apoptosis was detected using an Annexin V-FITC/7-AAD apoptosis detection kit (cat. no. 40311ES60; Shanghai Yeasen Biotechnology Co., Ltd.) according to the manufacturer's instructions. Briefly, cells were collected by trypsinization and resuspended in 500 μl binding buffer. The cell suspension was stained with 5 μl Annexin V-FITC and 5 μl 7-AAD for 5 min at room temperature in the dark. Samples were immediately analyzed using a CytoFLEX flow cytometer (Beckman Coulter, Inc.). Unstained cells were included as negative controls. Flow cytometry data were subsequently analyzed using FlowJo software (version 10.8.1; FlowJo LLC).

Western blotting. Total proteins were extracted using RIPA buffer (cat. no. P0013B; Beyotime Institute of Biotechnology) supplemented with PMSF (cat. no. ST2573; Beyotime Institute of Biotechnology), whereas nuclear proteins were isolated using a Nuclear and Cytoplasmic Protein Extraction Kit (cat. no. P0027; Beyotime Institute of Biotechnology). Protein concentrations were measured using a BCA Protein Assay Kit (cat. no. P0009; Beyotime Institute of Biotechnology). Equal amounts of proteins (30 μg) were separated by 10% SDS-PAGE and transferred onto PVDF membranes. After blocking with 5% bovine serum albumin (BSA; cat. no. ST023; Beyotime Institute of Biotechnology) for 1 h, the membranes were incubated overnight at 4˚C with primary antibodies against β-catenin (1:1,000; cat. no. ab32572; Abcam), NEK2 (1:1,000; cat. no. ab227958; Abcam), HIF-1α (1:1,000; cat. no. 20960-1-AP; Proteintech Group, Inc.), SLC7A11 (1:1,000; cat. no. 26864-1-AP; Proteintech Group, Inc.), GAPDH (1:1,000; cat . no. ab8245; Abcam), Lamin B (1:1,000; cat. no. ab133741; Abcam), Bcl-2 (1:1,000; cat. no. 12789-1-AP; Proteintech Group, Inc.), Bax (1:1,000; cat. no. 60267-1-Ig; Proteintech Group, Inc.), caspase-3 (1:1,000; cat. no. ab184787; Abcam) and GPX4 (1:1,000; cat. no. 59735; Cell Signaling Technology, Inc.). After washing with Tris-buffered saline containing 0.1% Tween-20 (TBST), the membranes were incubated with HRP-conjugated secondary antibodies (1:5,000; cat. no. A0208/A0216; Beyotime Institute of Biotechnology) for 1 h at room temperature. Protein bands were visualized using BeyoWB™ 30 min Western Assay Kit (cat. no. P0001M; Beyotime Institute of Biotechnology) and quantified by ImageJ software (version 1.53; National Institutes of Health).

TOPFlash/FOPFlash reporter assay. β-catenin transcriptional activity was assessed using TOPFlash/FOPFlash reporter assays. GC cells were co-transfected with TOPFlash (cat. no. 12456; Addgene, Inc.) or FOPFlash (cat. no. 12457; Addgene, Inc.) reporter plasmids and a *Renilla* luciferase plasmid using Lipofectamine™ 2000. At 24 h post-transfection, firefly and *Renilla* luciferase activities were measured using the Dual-Luciferase® Reporter Assay System (cat. no. E1910; Promega Corporation). Firefly luciferase activity was normalized to *Renilla* luciferase activity, and the results were expressed relative to the control group.

Measurement of GSH and oxidized glutathione (GSSG) levels. Total glutathione and GSSG levels were measured using a GSH/GSSG Detection Kit (cat. no. S0053; Beyotime Institute of Biotechnology) according to the manufacturer's instructions. Briefly, prepared samples or standards were mixed with glutathione detection working solution and incubated at room temperature for 5 min. NADPH solution was then added to initiate the enzymatic reaction, followed by incubation for 25 min. Absorbance at 412 nm was measured using a microplate reader. For GSSG measurement, endogenous GSH was removed from parallel samples before detection. GSH levels were calculated by subtracting GSSG from total glutathione.

GPX4 activity assay. GPX4 activity was measured using a Glutathione Peroxidase 4 Activity Assay Kit (cat. no. E-BC-K883-M; Wuhan Elabscience Biotechnology Co., Ltd.) according to the manufacturer's instructions. Briefly, ~$1x10^6$ cells were homogenized in ice-cold extraction buffer and centrifuged at 10,000 x g for 10 min at 4˚C. The supernatant was collected for enzymatic activity measurement, and protein concentration was determined using a BCA Protein Assay Kit (cat. no. E-BC-K318-Ml Wuhan Elabscience Biotechnology Co., Ltd.). Absorbance at 340 nm was recorded

using a microplate reader. GPX4 activity was calculated according to the manufacturer's formula and normalized to protein concentration. Results were expressed as U/g protein.

Flow cytometric analysis of lipid peroxidation and reactive oxygen species (ROS). Lipid peroxidation and intracellular ROS levels were analyzed by flow cytometry using BODIPY™ 581/591 C11 and CM-H2DCFDA probes, respectively. Briefly, $1x10^6$ cells were harvested, washed with PBS, and incubated in serum-free medium containing BODIPY™ 581/591 C11 (5 μM; cat. no. D3861; Invitrogen; Thermo fisher Scientific, Inc.) or CM-H2DCFDA (5 μM; cat. no. D6470; Beijing Solarbio Science & Technology Co., Ltd.). Probe incubation was performed at 37˚C for 20 min. After incubation, cells were washed three times with serum-free medium, resuspended in PBS, and immediately analyzed using a CytoFLEX flow cytometer (Beckman Coulter, Inc.).

Malondialdehyde (MDA) assay. MDA levels were quantified using a Lipid Peroxidation MDA Assay Kit (cat. no. S0131S; Beyotime Institute of Biotechnology) according to the manufacturer's instructions. Briefly, $5x10^6$ cells were lysed, and protein concentration was determined using a BCA Protein Assay Kit (cat. no. P0009; Beyotime Institute of Biotechnology). Cell lysates, blanks, or MDA standards were mixed with chromogenic reagent and heated in a boiling-water bath for 15 min. After rapid cooling and centrifugation at 1,000 x g for 10 min, the supernatant was collected, and absorbance at 532 nm was measured. MDA levels were calculated from the standard curve and normalized to protein concentration. Results were expressed as μmol/g protein.

Calcein-AM/propidium iodide (PI) live/dead staining. Live and dead cells were assessed using a Calcein AM/PI Double Staining Kit (cat. no. 40747ES76; Shanghai Yeasen Biotechnology Co., Ltd.) according to the manufacturer's instructions. Briefly, cells were collected, washed with 1X assay buffer, and resuspended at $1x10^6$ cells/ml. The cell suspension was mixed with Calcein-AM/PI working solution containing 2 μM Calcein-AM and 4.5 μM PI. After incubation at 37˚C for 15 min in the dark, cells were immediately analyzed using a CytoFLEX flow cytometer (Beckman Coulter, Inc.).

Chromatin Immunoprecipitation (ChIP)-qPCR assay. AGS cells were transfected with siNC, siNEK2, or siNEK2 together with an HIF1A overexpression plasmid. Chromatin immunoprecipitation was performed using the SimpleChIP Enzymatic Chromatin IP Kit (cat. no. 9003; Cell Signaling Technology, Inc.) according to the manufacturer's instructions. Briefly, cells were cross-linked, lysed, and subjected to chromatin fragmentation. The fragmented chromatin was immunoprecipitated using an anti-HIF-1α antibody (cat. no. 36169; Cell Signaling Technology, Inc.), with normal rabbit IgG (cat. no. 2729; Cell Signaling Technology, Inc.) serving as a negative control. Following reversal of cross-links and DNA purification, immunoprecipitated DNA was analyzed by ChIP-qPCR targeting the HIF-1α-binding region within the SLC7A11 promoter. The primers were as follows: forward, 5'-TCCCTT CTTTCCCTGCCAAC-3' and reverse, 5'-CCCTGAAGCTAC CTTTATACGCA-3'.

Dual-luciferase reporter assay. The wild-type (WT) SLC7A11 promoter sequence and its corresponding mutant (MT) sequence were cloned into the pGL3-Basic firefly luciferase reporter vector (cat. no. E1751; Promega Corporation). AGS cells were co-transfected with WT or MT reporter plasmids, a *Renilla* luciferase internal control plasmid, and siNC, siNEK2, or siNEK2 together with a β-catenin overexpression plasmid using Lipofectamine™ 2000. After 24 h, cells were lysed, and firefly and *Renilla* luciferase activities were measured using the Dual-Luciferase Reporter Assay System (cat. no. E1910; Promega Corporation). Firefly luciferase activity was normalized to *Renilla* luciferase activity.

Intracellular Fe^{2+} detection. Intracellular ferrous iron (Fe^{2+}) levels were detected using the FeRhoNox™-1 fluorescent probe. Following the indicated treatments, AGS cells were washed twice with PBS and incubated with FeRhoNox™-1 (5 μM; cat. no. GC901; Goryo Chemical, Inc.) at 37˚C for 60 min in the dark. After washing with PBS, cell nuclei were counterstained with DAPI (1 μg/ml), and fluorescence images were captured using a fluorescence microscope. Relative FeRhoNox™-1 fluorescence intensity was quantified using ImageJ software.

Statistical analysis. Data are presented as the mean ± standard deviation (SD). Statistical analyses were performed using SPSS 22.0 software (IBM Corp.). IC_{50} and IC_{20} values were estimated using a Logit model. Multiple-group comparisons were performed using one-way analysis of variance (ANOVA) followed by Tukey's honestly significant difference test. All statistical tests were two-tailed, and $P<0.05$ was considered to indicate a statistically significant difference.

Results

NEK2 knockdown enhances OXA-induced growth inhibition and cell death in GC cells. To establish appropriate OXA treatment conditions, the sensitivity of AGS and HGC-27 cells to OXA was first assessed. Treatment with increasing concentrations of OXA (0, 0.5, 2, 8, 32 and 128 μM) for 24 h reduced cell viability in a concentration-dependent manner, yielding IC_{50} values of 12.1 and 6.2 μM, respectively (Fig. 1A and B). Based on these dose-response curves, OXA concentrations corresponding to the IC_{20} values (6.5 μM for AGS cells and 2.3 μM for HGC-27 cells) were selected for subsequent experiments.

It was next investigated whether NEK2 knockdown enhances the inhibitory effects of OXA on GC cells. After confirming NEK2 knockdown by RT-qPCR (Fig. 1C), it was found that NEK2 silencing further reduced cell viability in both AGS and HGC-27 cells under OXA treatment compared with OXA treatment alone (Fig. 1D and E). To further address potential siRNA off-target effects, two independent NEK2-targeting siRNAs were tested in AGS cells. Both siNEK2#1 and siNEK2#2 further reduced cell viability under OXA treatment (Fig. 1F). Consistently, NEK2 knockdown further decreased EdU incorporation and increased apoptosis in OXA-treated cells (Fig. 1G-J). Collectively, these results indicate that NEK2 knockdown enhances OXA-induced growth inhibition and cell death in GC cells.

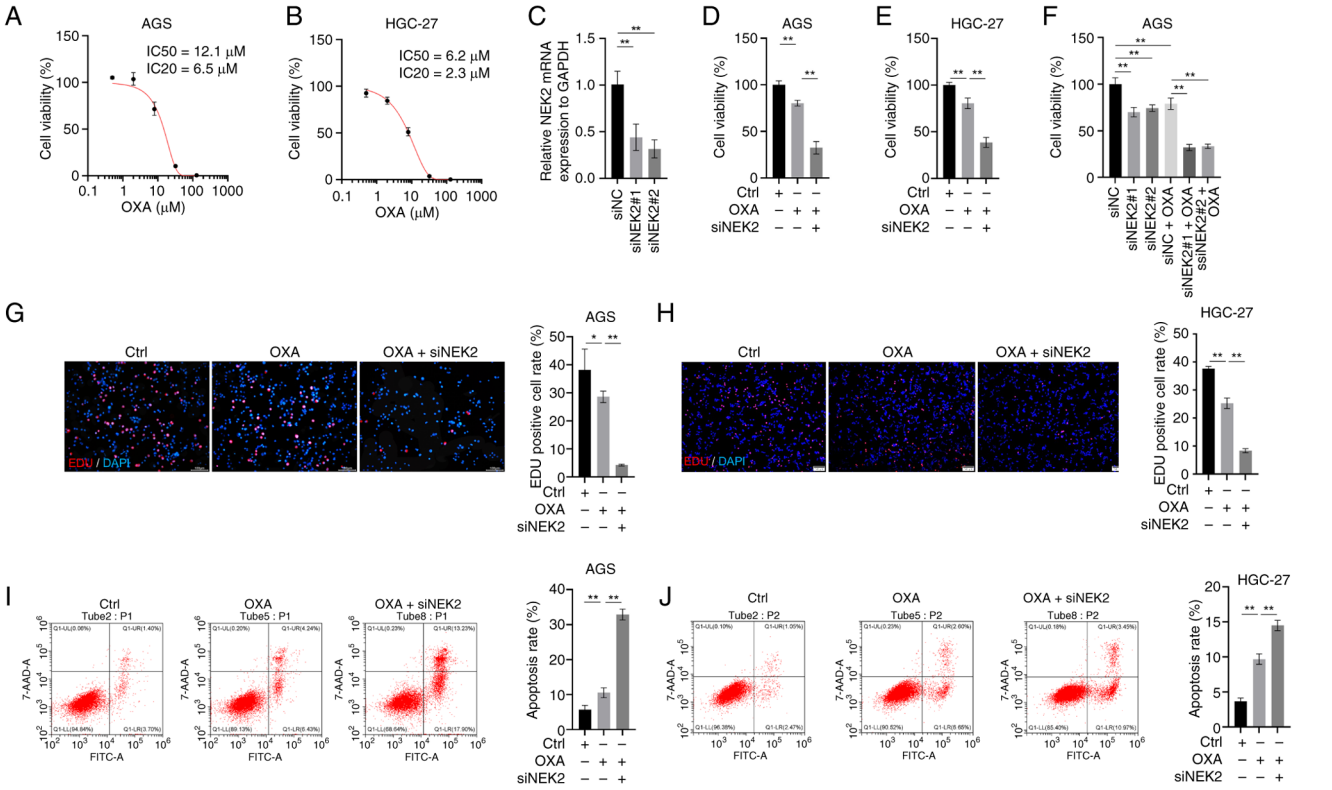

Figure 1. NEK2 knockdown enhances OXA-induced growth inhibition and cell death in gastric cancer cells. (A and B) AGS and HGC-27 cells were exposed to increasing concentrations of OXA (0, 0.5, 2, 8, 32 and 128 μM) for 24 h, after which cell viability was measured using the CCK-8 assay. IC_{50} and IC_{20} values were calculated using a Logit model. (C) NEK2 knockdown efficiency was assessed by reverse transcription-quantitative PCR. (D and E) AGS and HGC-27 cells were transfected with siNEK2 or negative control siRNA (siNC) for 72 h and subsequently exposed to OXA (6.5 μM for AGS and 2.3 μM for HGC-27) for 24 h, and cell viability was determined by the CCK-8 assay. (F) AGS cells were transfected with siNC, siNEK2#1, or siNEK2#2 for 72 h, followed by treatment with or without OXA (6.5 μM) for 24 h. Cell viability was determined using the CCK-8 assay. (G and H) DNA synthesis was evaluated by the EdU incorporation assay, and the percentage of EdU-positive cells was quantified. Scale bar, 100 μm. (I and J) Apoptosis was quantified by Annexin V-FITC/7-AAD staining and flow cytometry. Data are presented as the mean ± SD. Statistical significance was determined by one-way ANOVA followed by Tukey's post hoc test; *P<0.05 and **P<0.01; n=3. NEK2, NIMA-related kinase 2; OXA, oxaliplatin; si-, small interfering; NC, negative control; CCK-8, Cell Counting Kit-8; Ctrl, control.

NEK2 promotes HIF-1α/SLC7A11 signaling through β-catenin activation. To investigate the molecular mechanism underlying NEK2-mediated regulation of OXA responsiveness, HIF-1α/SLC7A11 signaling was first examined. NEK2 knockdown significantly reduced HIF-1α and SLC7A11 expression at both the mRNA and protein levels (Fig. 2A-D). Moreover, HIF-1α overexpression partially restored SLC7A11 protein expression in NEK2-knockdown cells (Fig. 2E and F). ChIP-qPCR further revealed that NEK2 knockdown decreased HIF-1α binding to the SLC7A11 promoter, whereas HIF-1α overexpression partially restored this enrichment (Fig. 2G). Collectively, these findings suggest that HIF-1α contributes to the regulation of SLC7A11 expression downstream of NEK2.

To further elucidate the mechanism by which NEK2 regulates HIF-1α/SLC7A11 signaling, focus was addressed on β-catenin. Previous studies have shown that NEK2 activates β-catenin signaling (27,28) and that β-catenin promotes HIF-1α expression (29). NEK2 knockdown reduced total and nuclear β-catenin protein levels (Fig. 2H and I) and suppressed β-catenin transcriptional activity, as assessed by TOPFlash/FOPFlash reporter assays (Fig. 2J and K). To determine whether β-catenin mediates NEK2-dependent regulation of HIF-1α/SLC7A11 signaling, β-catenin was overexpressed in NEK2-knockdown cells. β-catenin overexpression restored its nuclear abundance and transcriptional activity (Fig. 2L-N), accompanied by partial restoration of HIF-1α and SLC7A11 protein expression (Fig. 2O). Furthermore, NEK2 knockdown decreased WT SLC7A11 promoter activity, which was partially restored by β-catenin overexpression. Notably, these effects were abolished when the HIF-1α-binding site was mutated (Fig. 2P). Collectively, these findings indicate that NEK2 promotes HIF-1α/SLC7A11 signaling through β-catenin activation.

Restoration of HIF-1α attenuates NEK2 knockdown-enhanced OXA responsiveness. To determine whether HIF-1α is involved in the regulation of OXA responsiveness by NEK2, rescue experiments were performed. Compared with OXA treatment alone, NEK2 knockdown further intensified the effects of OXA treatment, leading to reduced cell viability and EdU incorporation and increased apoptosis. Notably, HIF-1α overexpression partially reversed these effects (Fig. 3A-C). In agreement with these findings, NEK2 knockdown further decreased Bcl-2 expression and increased Bax expression and caspase-3 cleavage in OXA-treated cells. These changes were partially attenuated by HIF-1α overexpression (Fig. 3D). Collectively, these results suggest that HIF-1α restoration

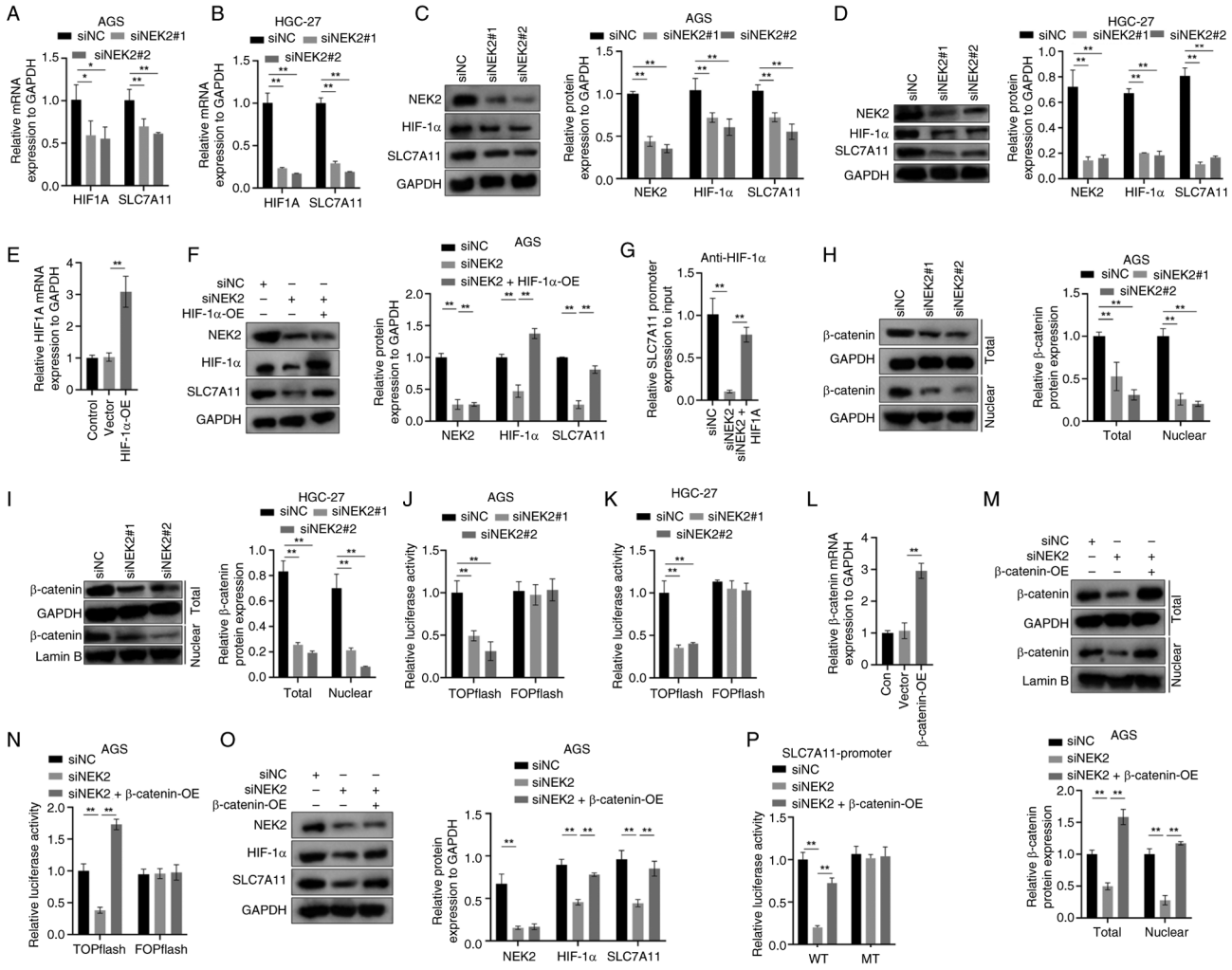

Figure 2. NEK2 promotes HIF-1α/SLC7A11 signaling through β-catenin activation. (A-D) AGS and HGC-27 cells were transfected with siNEK2 or siNC for 72 h. (A and B) HIF-1α and SLC7A11 mRNA expression levels were quantified by RT-qPCR. (C and D) NEK2, HIF-1α and SLC7A11 protein levels were analyzed by western blotting. (E) HIF-1α overexpression efficiency was confirmed by RT-qPCR. (F) AGS cells were transfected with siNEK2 or siNC, with or without an HIF-1α overexpression vector, for 72 h. NEK2, HIF-1α and SLC7A11 protein levels were analyzed by western blotting. (G) Chromatin immunoprecipitation-quantitative PCR was performed using an anti-HIF-1α antibody to evaluate HIF-1α binding to the SLC7A11 promoter in AGS cells following NEK2 knockdown with or without HIF-1α overexpression. (H and I) Total and nuclear β-catenin levels were examined by western blotting. (J and K) β-catenin transcriptional activity was evaluated using TOPFlash and FOPFlash luciferase reporter assays. (L) β-catenin overexpression efficiency was confirmed by RT-qPCR. (M and O) AGS cells were transfected with siNEK2 or siNC, with or without a β-catenin overexpression vector, for 72 h. (M) Total and nuclear β-catenin levels were assessed by western blotting. (N) β-catenin transcriptional activity was measured using TOPFlash/FOPFlash reporter assays. (O) NEK2, HIF-1α and SLC7A11 protein levels were analyzed by western blotting. (P) Dual-luciferase reporter assays were performed in AGS cells using WT or MT SLC7A11 promoter vectors following NEK2 knockdown with or without β-catenin overexpression. Data are presented as the mean ± SD. Statistical significance was determined by one-way ANOVA followed by Tukey's post hoc test. *P<0.05 and **P<0.01; n=3. NEK2, NIMA-related kinase 2; HIF-1α, hypoxia-inducible factor 1α; SLC7A11, solute carrier family 7 member 11; si-, small interfering; NC, negative control; RT-qPCR, reverse transcription-quantitative PCR; WT, wild-type; MT, mutant; OE, overexpression.

partially counteracts the enhanced OXA responsiveness induced by NEK2 knockdown, supporting a role for HIF-1α in NEK2-mediated regulation of OXA responsiveness.

NEK2 sustains GSH/GPX4-dependent antioxidant defense through HIF-1α/SLC7A11 signaling. Given that HIF-1α overexpression attenuated the enhanced OXA responsiveness caused by NEK2 knockdown, it was next sought to elucidate the underlying mechanism. Previous studies reported that HIF-1α promotes SLC7A11 expression, thereby supporting cystine uptake and GSH synthesis, while GSH serves as an essential substrate for GPX4-mediated detoxification of lipid peroxides. It was therefore examined whether NEK2 regulates GSH/GPX4-dependent antioxidant defense system. In both AGS and HGC-27 cells, NEK2 knockdown decreased intracellular GSH and increased GSSG levels (Fig. 4A and B). Consistently, GPX4 protein expression and enzymatic activity were reduced following NEK2 knockdown (Fig. 4C-F). To assess the contribution of HIF-1α to these changes, HIF-1α was overexpressed in AGS cells following NEK2 knockdown. HIF-1α overexpression partially restored GSH levels, attenuated GSSG accumulation, and increased GPX4 protein expression and enzymatic activity (Fig. 4G-I), suggesting that HIF-1α contributes to the maintenance of GSH/GPX4-dependent antioxidant defense downstream of NEK2. It was next investigated whether HIF-1α also mediates the increase in intracellular Fe^{2+} associated with NEK2 knockdown. A previous study by the authors showed that NEK2 knockdown promotes Fe^{2+}

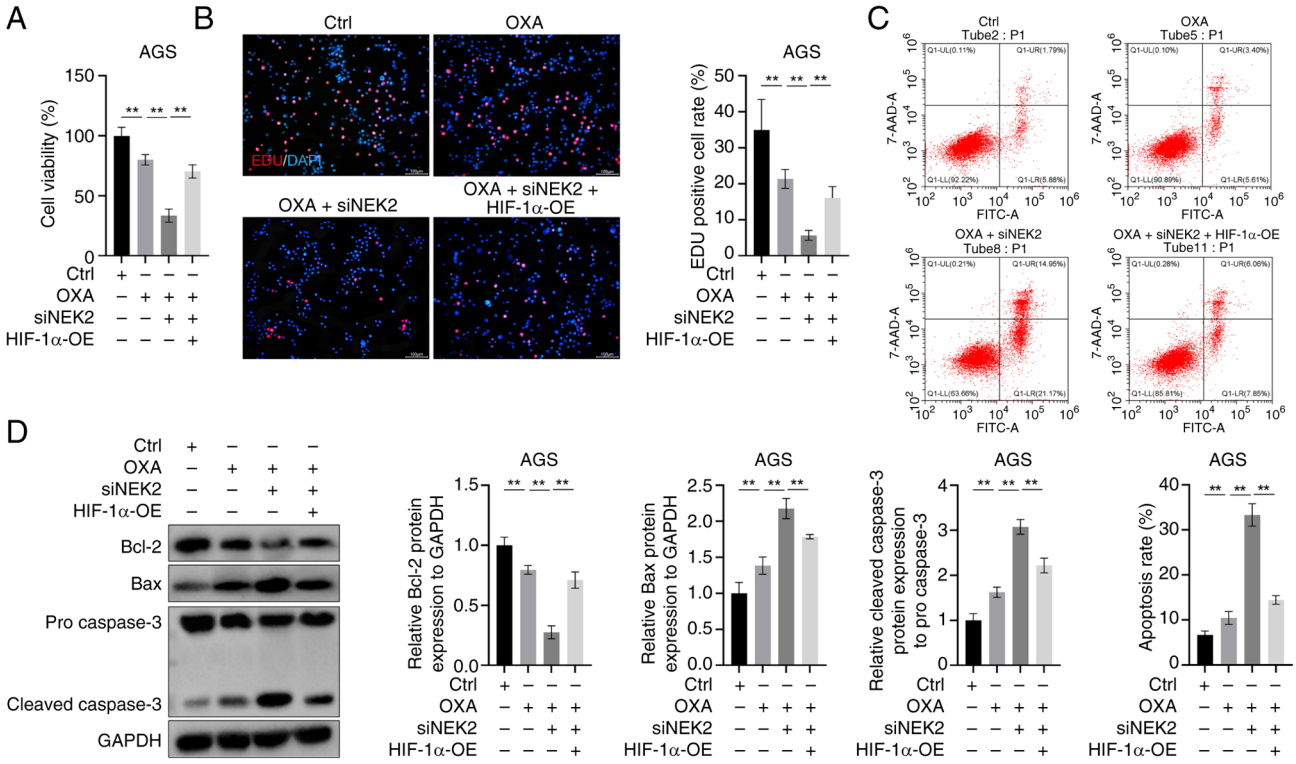

Figure 3. Restoration of HIF-1α attenuates NEK2 knockdown-enhanced OXA responsiveness. (A-D) AGS cells were transfected with siNEK2 or siNC, in the presence or absence of an HIF-1α overexpression vector, for 72 h followed by treatment with OXA (6.5 μM) for 24 h. (A) Cell viability was determined by the Cell Counting Kit-8 assay. (B) DNA synthesis was evaluated by the EdU incorporation assay. (C) Apoptosis was quantified by Annexin V-FITC/7-AAD staining. (D) Bcl-2, Bax, pro-caspase-3 and cleaved caspase-3 protein levels were analyzed by western blotting. Data are presented as the mean ± SD. Statistical significance was determined by one-way ANOVA followed by Tukey's post hoc test. **P<0.01; n=3. HIF-1α, hypoxia-inducible factor 1α; NEK2, NIMA-related kinase 2; OXA, oxaliplatin; OE, overexpression; si-, small interfering; Ctrl, control.

accumulation through Keap1/Nrf2/HMOX1 signaling (18). Consistent with this finding, NEK2 knockdown increased intracellular Fe^{2+} levels; however, HIF-1α overexpression did not reverse this increase (Fig. 4J). Collectively, these results suggest that NEK2 supports GSH/GPX4-dependent antioxidant defense, at least in part, through HIF-1α/SLC7A11 signaling, whereas Fe^{2+} accumulation induced by NEK2 knockdown appears to occur independently of HIF-1α.

NEK2 knockdown enhances ferroptosis susceptibility by suppressing HIF-1α/SLC7A11. Given the role of the GSH/GPX4 antioxidant system in protecting cells from ferroptosis through lipid peroxide detoxification (30), it was next investigated whether NEK2 knockdown affects ferroptosis susceptibility by impairing HIF-1α/SLC7A11-dependent GSH/GPX4 antioxidant defense. To address this, AGS cells were treated with the ferroptosis inducers RSL3 or FIN56, and the effects of HIF-1α overexpression were assessed in the context of NEK2 knockdown. Both treatments reduced intracellular GSH levels and GPX4 protein expression and enzymatic activity, while increasing GSSG levels. These effects were further enhanced by NEK2 knockdown but attenuated by HIF-1α overexpression (Fig. 5A-C). In line with this disruption of antioxidant defense, NEK2 knockdown further increased RSL3- and FIN56-induced ROS accumulation, MDA levels and lipid peroxidation, whereas HIF-1α overexpression alleviated these changes (Fig. 5D-F). It was next assessed whether these changes in oxidative stress were accompanied by increased cell death. NEK2 knockdown further reduced cell viability and increased cell death following RSL3 or FIN56 treatment, whereas HIF-1α overexpression partially reversed these effects (Fig. 5G and H). Collectively, these findings indicate that NEK2 knockdown enhances ferroptosis susceptibility in GC cells by weakening HIF-1α/SLC7A11-dependent GSH/GPX4 antioxidant defense.

NEK2 knockdown exacerbates OXA-induced ferroptosis-related oxidative damage by suppressing HIF-1α/SLC7A11 signaling. Having shown that NEK2 knockdown impairs HIF-1α/SLC7A11-associated GSH/GPX4 antioxidant defense and increases ferroptosis susceptibility, it was next investigated whether this mechanism contributes to OXA-induced ferroptosis-related oxidative damage. In AGS cells, OXA treatment decreased GSH levels, increased GSSG levels, and reduced GPX4 protein expression and enzymatic activity. Notably, NEK2 knockdown further aggravated these changes, whereas HIF-1α overexpression partially restored GSH levels, GPX4 expression and enzymatic activity while attenuating GSSG accumulation (Fig. 6A-C). In parallel, NEK2 knockdown further exacerbated OXA-induced increases in ROS accumulation, MDA levels and lipid peroxidation, whereas HIF-1α overexpression attenuated these effects (Fig. 6D-F). Taken together, these findings indicate that NEK2 knockdown exacerbates OXA-induced ferroptosis-related oxidative damage by weakening HIF-1α/SLC7A11-dependent GSH/GPX4 antioxidant defense.

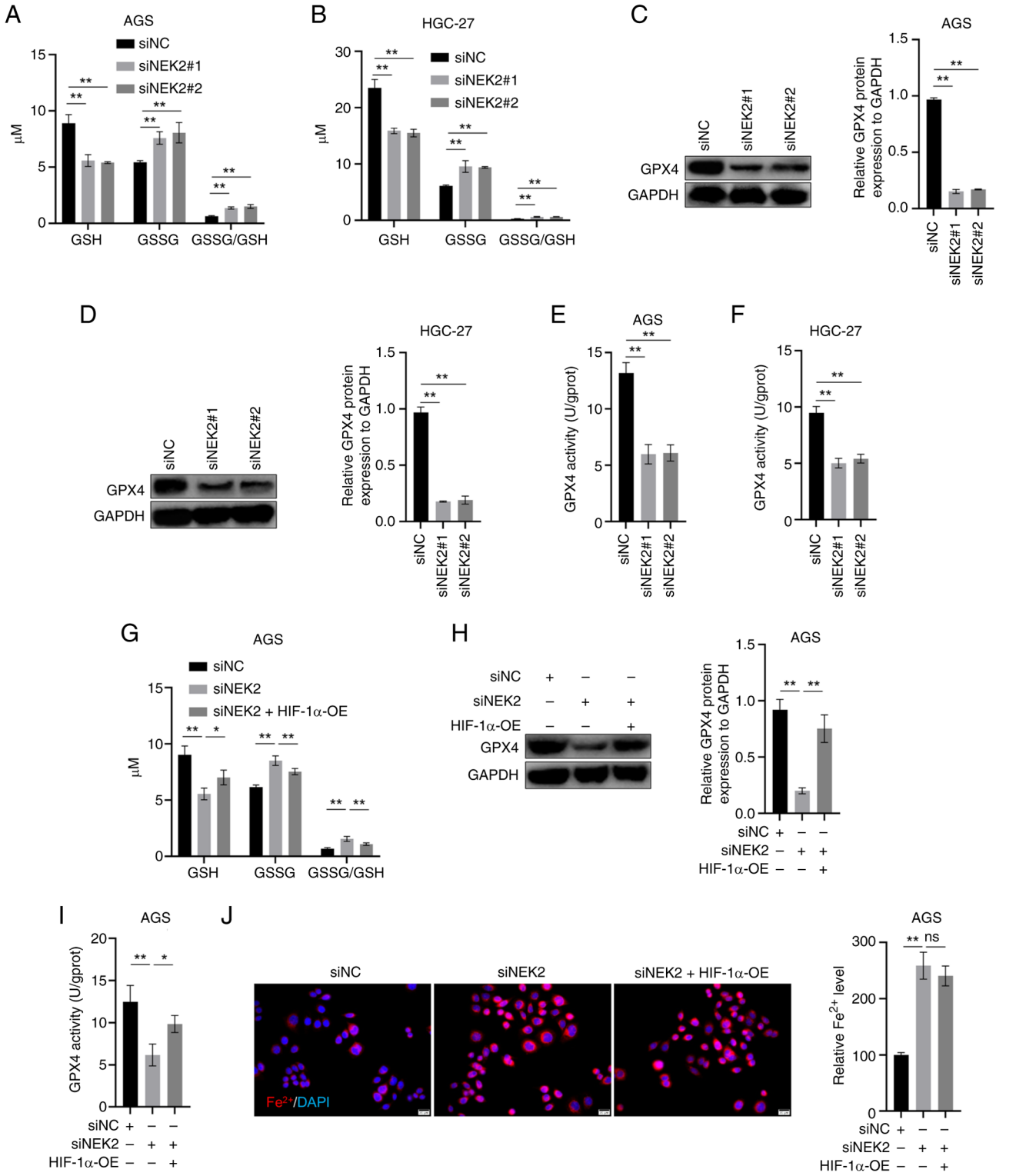

Figure 4. NEK2 sustains GSH/GPX4-dependent antioxidant defense through HIF-1α/SLC7A11 signaling. (A and B) AGS (A) and HGC-27 (B) cells were transfected with siNC, siNEK2#1, or siNEK2#2 for 72 h. Intracellular GSH and GSSG levels were measured using commercial assay kits. (C and D) GPX4 protein expression was analyzed by western blotting. (E and F) GPX4 activity was measured and quantitatively analyzed. (G) Intracellular GSH and GSSG levels were measured using a commercial assay kit. (H) GPX4 protein levels were analyzed by western blotting. (I) GPX4 activity was measured and quantitatively analyzed. (J) Representative fluorescence images and quantitative analysis of intracellular Fe^{2+} levels in AGS cells. Scale bar, 20 μm. Data are presented as the mean ± SD. Statistical significance was determined by one-way ANOVA followed by Tukey's post hoc test. *P<0.05 and **P<0.01; n=3. NEK2, NIMA-related kinase 2; GSH, glutathione; GPX4, glutathione peroxidase 4; HIF-1α, hypoxia-inducible factor 1α; SLC7A11, solute carrier family 7 member 11; si-, small interfering; NC, negative control; GSSG, oxidized glutathione; OE, overexpression; ns, not significant.

Ferroptosis inhibition attenuates NEK2 knockdown-enhanced OXA responsiveness in GC cells. To determine whether ferroptosis contributes to the increased OXA responsiveness induced by NEK2 knockdown, the effects of ferroptosis inhibitors Fer-1 and liproxstatin-1 were evaluated in OXA-treated AGS cells. As expected, NEK2 knockdown further reduced

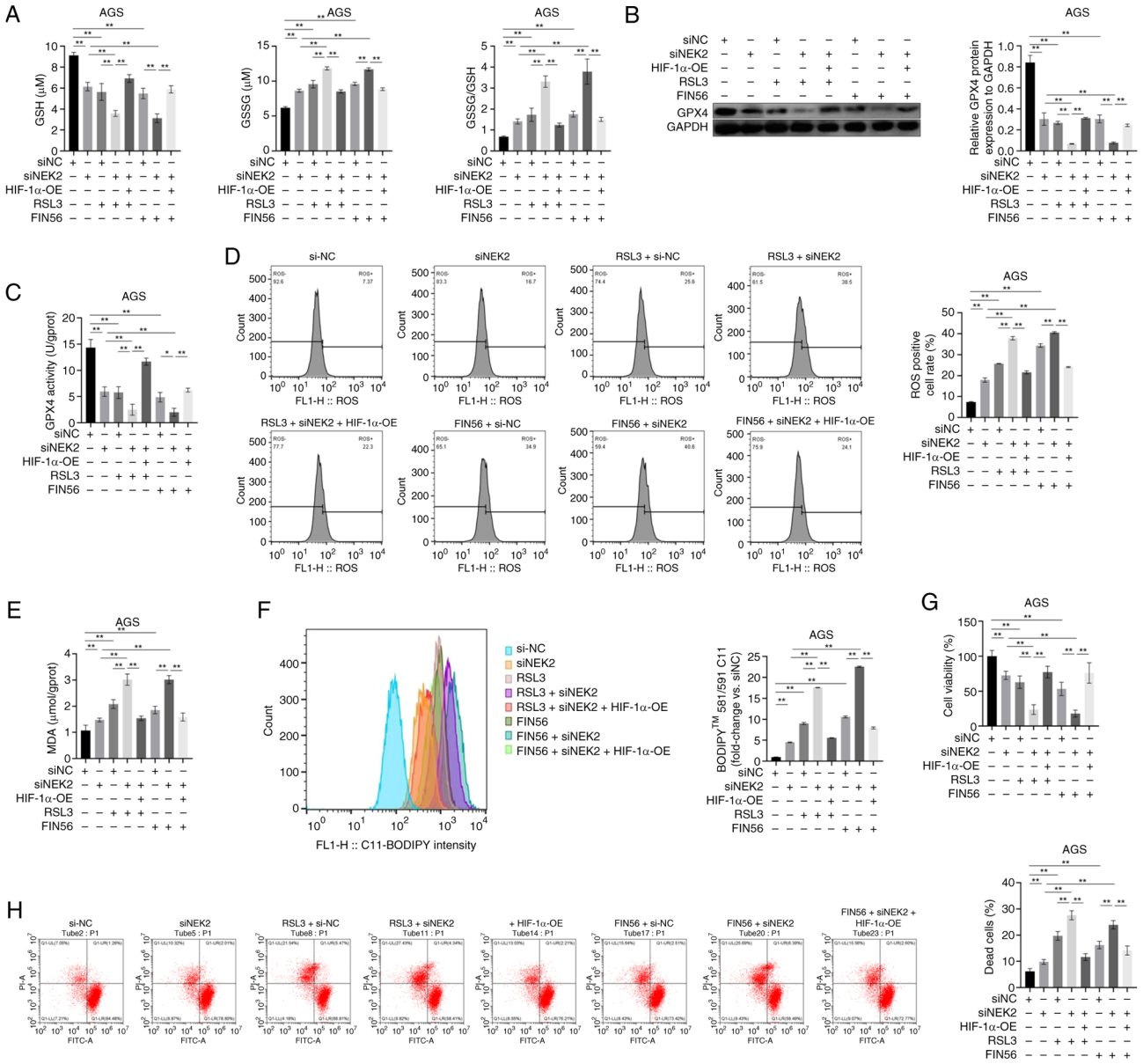

Figure 5. NEK2 knockdown enhances ferroptosis susceptibility by suppressing HIF-1α/SLC7A11. (A-H) AGS cells were transfected with siNEK2 or siNC, with or without an HIF-1α overexpression vector, for 72 h and then treated with RSL3 (2 μM) or FIN56 (5 μM) for 12 h. (A) Intracellular GSH and GSSG levels were measured using a commercial assay kit. (B) GPX4 protein levels were analyzed by western blotting. (C) GPX4 activity was measured and quantitatively analyzed. (D) Intracellular reactive oxygen species levels were detected using CM-H2DCFDA. (E) MDA levels were quantified using a commercial assay kit. (F) Lipid peroxidation was assessed using the BODIPY™ 581/591 C11 probe. (G) Cell viability was determined by the Cell Counting Kit-8 assay. (H) Live/dead cell ratios were analyzed by Calcein-AM/propidium iodide staining. Data are presented as the mean ± SD. Statistical significance was determined by one-way ANOVA followed by Tukey's post hoc test. *P<0.05 and **P<0.01; n=3. NEK2, NIMA-related kinase 2; HIF-1α, hypoxia-inducible factor 1α; SLC7A11, solute carrier family 7 member 11; si-, small interfering; NC, negative control; GSH, glutathione; GSSG, oxidized glutathione; GPX4, glutathione peroxidase 4; MDA, malondialdehyde; OE, overexpression.

cell viability and EdU incorporation while increasing apoptosis under OXA treatment. Importantly, both Fer-1 and liproxstatin-1 partially restored cell viability and EdU incorporation and attenuated the increase in apoptosis (Fig. 7A-C). Collectively, these findings support a functional contribution of ferroptosis to the enhanced OXA responsiveness following NEK2 knockdown in GC cells.

Discussion

Although OXA-based chemotherapy remains a cornerstone of treatment for advanced GC, suboptimal therapeutic responses and the emergence of drug resistance continue to compromise its clinical efficacy. An improved understanding of the molecular mechanisms underlying OXA responsiveness is crucial for identifying potential therapeutic targets and developing strategies to improve treatment outcomes. In the present study, it was found that NEK2 knockdown enhanced the inhibitory effects of OXA on GC cell proliferation and further increased OXA-induced apoptosis. Mechanistically, NEK2 knockdown suppressed HIF-1α/SLC7A11-dependent GSH/GPX4 antioxidant defense, disrupting cellular redox homeostasis and increasing susceptibility to ferroptosis. This impairment of antioxidant defense was accompanied by more pronounced

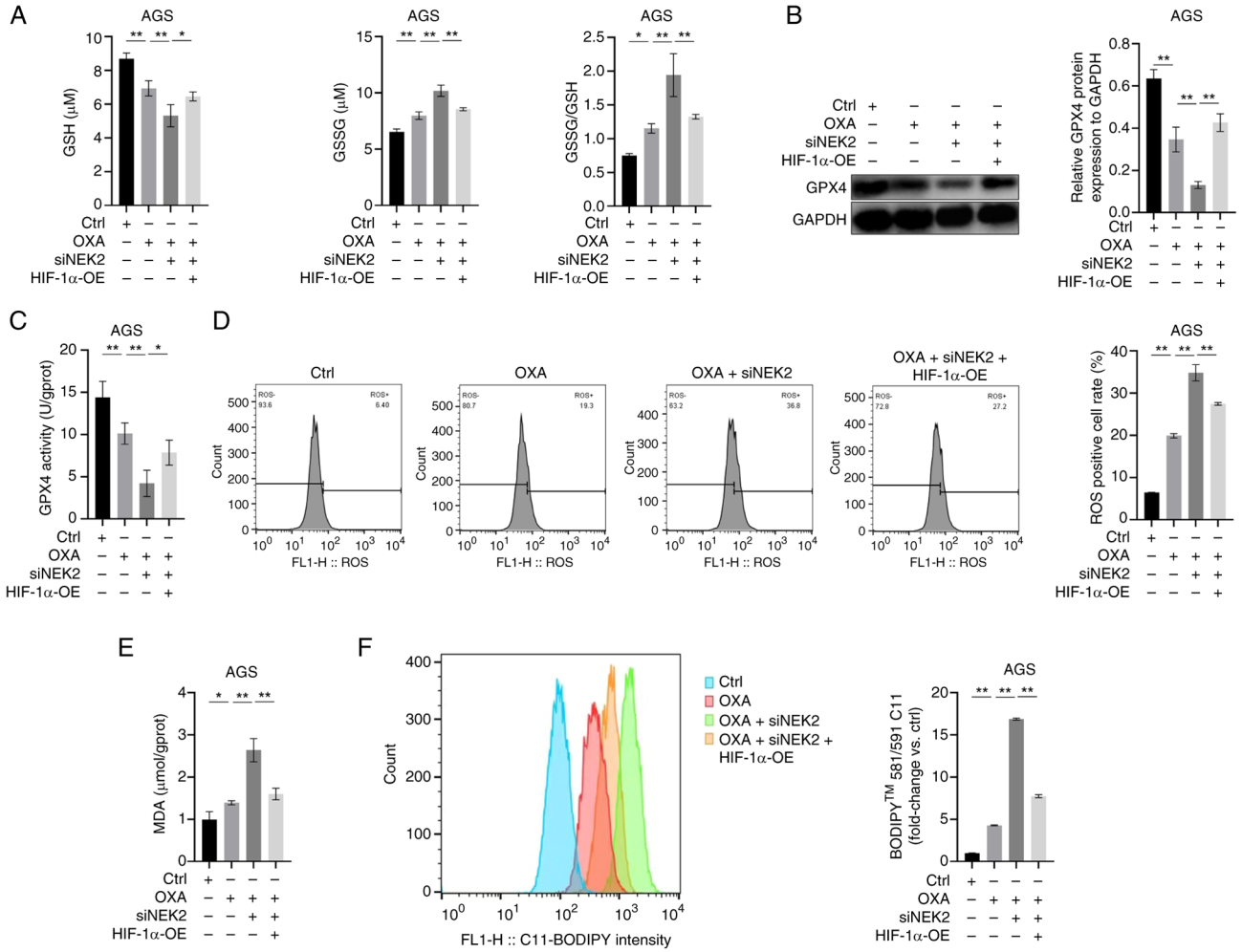

Figure 6. NEK2 knockdown exacerbates OXA-induced ferroptosis-related oxidative damage by suppressing HIF-1α/SLC7A11 signaling. (A-F) AGS cells were transfected with siNEK2 or siNC, in the presence or absence of an HIF-1α overexpression vector, for 72 h before being exposed to OXA (6.5 μM) for 24 h. (A) Intracellular GSH and GSSG levels were determined using a commercial assay kit. (B) GPX4 protein levels were analyzed by western blotting. (C) GPX4 activity was measured and quantitatively analyzed. (D) Intracellular reactive oxygen species levels were detected using CM-H2DCFDA. (E) MDA levels were quantified using a commercial assay kit. (F) Lipid peroxidation was assessed using the BODIPY™ 581/591 C11 probe. Data are presented as the mean ± SD. Statistical significance was determined by one-way ANOVA followed by Tukey's post hoc test. *P<0.05 and **P<0.01; n=3. NEK2, NIMA-related kinase; OXA, oxaliplatin; HIF-1α, hypoxia-inducible factor 1α; SLC7A11, solute carrier family 7 member 11; si-, small interfering; NC, negative control; GSH, glutathione; GSSG, oxidized glutathione; GPX4, glutathione peroxidase 4; MDA, malondialdehyde; OE, overexpression.

OXA-induced ferroptosis-related oxidative damage, as evidenced by increased ROS accumulation, MDA levels and lipid peroxidation. Moreover, restoration of HIF-1α expression partially alleviated the disruption of GSH/GPX4-dependent antioxidant defense and the associated oxidative damage. Importantly, pharmacological treatment with ferroptosis inhibitors partially reversed the enhanced OXA responsiveness caused by NEK2 knockdown. Collectively, these findings establish a functional link between NEK2-mediated antioxidant defense and the cellular response to OXA.

NEK2 has emerged as an important contributor to GC progression through oncogenic pathways, including AKT/HIF-1α signaling and β-catenin-associated transcriptional regulation (9,11,31). In a previous study by the authors, it was further demonstrated that NEK2 knockdown increased ferroptosis susceptibility through modulation of Keap1/Nrf2/HMOX1 signaling (18). Building on these findings, the present study provides further evidence of the role of NEK2 in GC by demonstrating that its knockdown enhances cellular responsiveness to OXA. These findings also highlight the potential translational relevance of targeting NEK2 to improve the efficacy of chemotherapy. In this context, T-1101 tosylate, a selective NEK2 inhibitor, has shown antitumor activity with limited toxicity and is currently under Phase I clinical evaluation (32). In addition, previous studies have reported that combining T-1101 and conventional chemotherapeutic agents, including doxorubicin, paclitaxel, or topotecan, enhances antitumor efficacy (33). Taken together, these findings provide a rationale for further investigation of NEK2 inhibition as a potential strategy to improve the therapeutic response to OXA-based chemotherapy in GC. However, the efficacy and safety of this combination will require further validation in appropriate preclinical models and, ultimately, clinical studies.

Additionally, the present study further implicates HIF-1α/SLC7A11 signaling as a potential mechanistic link between NEK2 and OXA responsiveness. It was observed that NEK2 knockdown decreased HIF-1α and SLC7A11 expression,

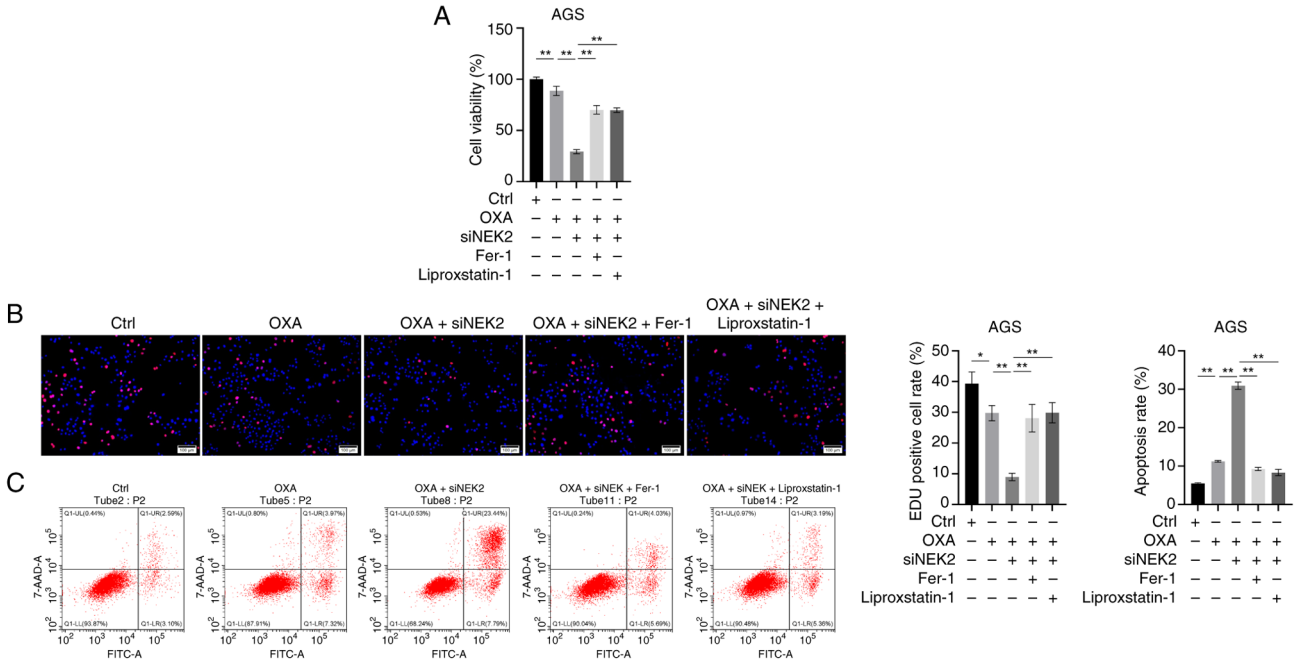

Figure 7. Ferroptosis inhibition attenuates NEK2 knockdown-enhanced OXA responsiveness in gastric cancer cells. (A-C) AGS cells were treated with OXA alone or in combination with NEK2 knockdown, with or without Fer-1 (2 μM) or liproxstatin-1 (1 μM). (A) Cell viability was assessed using the Cell Counting Kit-8 assay. (B) DNA synthesis was evaluated by the EdU incorporation assay, and the percentage of EdU-positive cells was quantified. Scale, 100 μm. (C) Apoptosis was assessed by Annexin V-FITC/7-AAD staining and flow cytometry. Data are presented as the mean ± SD. Statistical significance was determined by one-way ANOVA followed by Tukey's post hoc test. *P<0.05 and **P<0.01; n=3. NEK2, NIMA-related kinase; OXA, oxaliplatin; si-, small interfering.

whereas restoration of HIF-1α partially restored SLC7A11 expression and attenuated the enhanced OXA responsiveness induced by NEK2 knockdown. Moreover, ChIP-qPCR and promoter-reporter assays provided evidence supporting the involvement of HIF-1α-dependent transcriptional regulation of SLC7A11. These findings agree with previous studies showing that HIF-1α promotes SLC7A11 transcription in other malignancies (23,34). Regarding the upstream regulation of HIF-1α, previous studies have demonstrated that NEK2 activates β-catenin signaling through direct phosphorylation and promotion of nuclear translocation in GC and hepatocellular carcinoma (11,13), or through Wnt1-dependent mechanisms have been implicated in cervical cancer (28). In addition, β-catenin has been reported to positively regulate HIF-1α expression (35,36). Consistent with these findings, the results of the present study showed that NEK2 knockdown reduced the nuclear abundance of β-catenin and its transcriptional activity, while β-catenin overexpression partially restored HIF-1α and SLC7A11 expression. Collectively, these results support a model in which NEK2 promotes HIF-1α/SLC7A11 signaling, at least in part, through activation of β-catenin, thereby contributing to the regulation of OXA responsiveness in GC cells.

The GSH/GPX4 antioxidant defense system plays a central role in protecting cells against ferroptosis by limiting the accumulation of lipid peroxides (19). SLC7A11 contributes to this protective mechanism by promoting cystine uptake and supporting GSH biosynthesis, thereby sustaining GPX4-mediated detoxification of lipid peroxides (37,38). In the present study, NEK2 knockdown disrupted this antioxidant system, as evidenced by decreased intracellular GSH levels, increased GSSG accumulation, and reduced GPX4 protein expression and enzymatic activity. Importantly, HIF-1α overexpression partially reversed these changes, further implicating HIF-1α in the regulation of antioxidant defense downstream of NEK2. Consistent with this finding, NEK2 knockdown increased the susceptibility of GC cells to ferroptosis induced by RSL3 or FIN56, as reflected by more pronounced oxidative damage and cell death. These effects were partially alleviated by HIF-1α overexpression, supporting the contribution of HIF-1α-associated antioxidant regulation to ferroptosis susceptibility associated with NEK2 knockdown. In addition to its effect on the GSH/GPX4 antioxidant defense system, NEK2 knockdown increased intracellular Fe^{2+} levels, consistent with the authors' previous findings involving Keap1/Nrf2/HMOX1 signaling (18). However, the increase was not reversed by HIF-1α overexpression, suggesting that the HIF-1α/SLC7A11-dependent effects of NEK2 are primarily associated with GSH/GPX4 antioxidant regulation rather than the observed changes in intracellular Fe^{2+}.

The contribution of this antioxidant mechanism to OXA responsiveness is particularly relevant to recent findings on ferroptosis-associated chemoresistance in GC (39). It has been recently demonstrated that BASP1-AS1-mediated PCBP2 lactylation has been reported to suppress ferroptosis and promote OXA resistance (40). Similarly, EphA2/USP38-dependent stabilization of SLC7A11 and USP10/UGT8-mediated NRF2 signaling have been shown to reinforce antioxidant defense and reduce OXA sensitivity (16,17). Collectively, these findings suggest that enhanced ferroptosis resistance can compromise the antitumor efficacy of OXA, although the underlying regulatory pathways may differ. In the present study, OXA treatment disrupted GSH/GPX4-dependent antioxidant defense, as evidenced by decreased GSH levels, increased GSSG levels,

and reduced GPX4 protein expression and enzymatic activity, accompanied by increased ROS and lipid peroxidation. NEK2 knockdown further enhanced these changes, whereas HIF-1α overexpression partially restored antioxidant defense and attenuated ferroptosis-related oxidative damage. More importantly, treatment with the ferroptosis inhibitors Fer-1 and liproxstatin-1 partially restored cell viability and EdU incorporation and attenuated the increase in apoptosis in OXA-treated cells following NEK2 knockdown. These rescue experiments provide functional evidence that ferroptosis contributes, at least in part, to the enhanced OXA responsiveness induced by NEK2 knockdown. Together with the HIF-1α rescue experiments, these observations support a mechanism whereby NEK2 maintains HIF-1α/SLC7A11-dependent GSH/GPX4 antioxidant defense to protect GC cells against OXA-induced ferroptosis-related damage.

Despite these mechanistic insights, the relevance of this pathway to acquired OXA resistance and therapeutic responses *in vivo* remains unclear. The present study was conducted using parental GC cell lines rather than established OXA-resistant models; therefore, whether NEK2 knockdown can reverse resistance once it has developed remains to be determined. In addition, the absence of animal experiments and clinical validation limits the extent to which these findings can be extrapolated to tumor responses *in vivo* or to patients receiving OXA-based chemotherapy. Further studies using OXA-resistant models, animal experiments, and clinically characterized GC specimens will help establish the therapeutic relevance of targeting NEK2.

In conclusion, the findings of the present study demonstrated that NEK2 knockdown enhances OXA responsiveness in GC cells, at least in part, by impairing HIF-1α/SLC7A11-dependent GSH/GPX4 antioxidant defense, thereby increasing ferroptosis susceptibility and exacerbating OXA-induced ferroptosis-related oxidative damage. The partial reversal of these effects by HIF-1α overexpression and pharmacological ferroptosis inhibitors further supports the functional involvement of this pathway in OXA responsiveness. These results identify NEK2-mediated antioxidant defense as an important regulator of the cellular response to OXA and provide a rationale for further exploring NEK2-targeted strategies to improve OXA-based chemotherapy in GC.

Acknowledgements

Not applicable.

Funding

The present study was supported by The Science and Technology Program of Lishui: Lishui Public Welfare Technology Application Research Plan Project (grant no. 2023GYX68), the Zhejiang Medicine and Health Technology Plan (grant no. 2024KY1844) and Natural Science Foundation of Zhejiang (grant no. LBY21H160004).

Availability of data and materials

The data generated in the present study may be requested from the corresponding author.

Authors' contributions

LT, HS, HX, CJ, DW, ZS, JL, KY and JZ contributed to the study conception and design, prepared materials, and collected and analyzed data. LT and JZ confirm the authenticity of all the raw data. LT wrote the first draft of the manuscript. All authors commented on previous versions of the manuscript. All authors read and approved the final version of the manuscript.

Ethics approval and consent to participate

Not applicable.

Patient consent for publication

Not applicable.

Competing interests

The authors declare that they have no competing interests.

References

1. Bray F, Laversanne M, Sung H, Ferlay J, Siegel RL, Soerjomataram I and Jemal A: Global cancer statistics 2022: GLOBOCAN estimates of incidence and mortality worldwide for 36 cancers in 185 countries. CA Cancer J Clin 74: 229-263, 2024.
2. Lei P, Cao L, Zhang H, Fu J, Wei X, Zhou F, Cheng J, Ming J, Lu H and Jiang T: Polyene phosphatidylcholine enhances the therapeutic response of oxaliplatin in gastric cancer through Nrf2/HMOX1 mediated ferroptosis. Transl Oncol 43: 101911, 2024.
3. Shitara K, Fleitas T, Kawakami H, Curigliano G, Narita Y, Wang F, Wardhani SO, Basade M, Rha SY, Zamaniah WI, *et al*: Pan-Asian adapted ESMO clinical practice guidelines for the diagnosis, treatment and follow-up of patients with gastric cancer. ESMO Open 9: 102226, 2024.
4. Zhou B, Zhang S, Shen Z, Si Y, Luo T, Shen H, Wei W, Yang Q, Duan M, Wang Z, *et al*: RAD1 promotes oxaliplatin resistance in gastric cancer by reinforcing NRF2-driven antioxidant defense and DDR checkpoint signaling. Drug Resist Updat 87: 101417, 2026.
5. Chen Y, Mi Y, Tan S, Chen Y, Liu S, Lin S, Yang C, Hong W and Li W: CEA-induced PI3K/AKT pathway activation through the binding of CEA to KRT1 contributes to oxaliplatin resistance in gastric cancer. Drug Resist Updat 78: 101179, 2024.
6. Xia J, Zhao H, Edmondson JL, Koss B and Zhan F: Role of NEK2 in tumorigenesis and tumor progression. Trends Mol Med 31: 79-93, 2024.
7. Jiang Y, Wang Y, Su F, Hou Y, Liao W, Li B and Mao W: Insights into NEK2 inhibitors as antitumor agents: From mechanisms to potential therapeutics. Eur J Med Chem 286: 117287, 2025.
8. Fang Y, Kong Y, Xi J, Zhu M, Zhu T, Jiang T, Hu W, Ma M and Zhang X: Preclinical activity of MBM-5 in gastrointestinal cancer by inhibiting NEK2 kinase activity. Oncotarget 7: 79327-79341, 2016.
9. Wan H, Xu L, Zhang H, Wu F, Zeng W and Li T: High expression of NEK2 promotes gastric cancer progression via activating AKT signaling. J Physiol Biochem 77: 25-34, 2020.
10. Fan WD, Chen T and Liu PJ: NIMA related kinase 2 promotes gastric cancer cell proliferation via ERK/MAPK signaling. World J Gastroenterol 25: 2898-2910, 2019.
11. Li Y, Chen L, Feng L, Zhu M, Shen Q, Fang Y, Liu X and Zhang X: NEK2 promotes proliferation, migration and tumor growth of gastric cancer cells via regulating KDM5B/H3K4me3. Am J Cancer Res 9: 2364-2378, 2019.
12. White MC, Lange PT, Stewart J and Damania B: NEK2 drives pathogenesis, drug resistance, and LMP1 expression in EBV-positive non-Hodgkin lymphoma. Proc Natl Acad Sci USA 123: e2535550123, 2026.
13. Deng L, Sun J, Chen X, Liu L and Wu D: Nek2 augments sorafenib resistance by regulating the ubiquitination and localization of β-catenin in hepatocellular carcinoma. J Exp Clin Cancer Res 38: 316, 2019.

14. Haiye J, Xiangzhu W, Yunfei Z, Shumin G, Chang N, Yaohui J, Heng Y and Xinmin N: Overexpressed NEK2 contributes to progression and cisplatin resistance through activating the Wnt/β-catenin signaling pathway in cervical cancer. Cancer Cell Int 25: 45, 2025.
15. Zheng J and Conrad M: Ferroptosis: When metabolism meets cell death. Physiol Rev 105: 651-706, 2024.
16. Gan J, Zou Y, Xu H, Fan L, Leng W, Li K, Liu Q, Chen Y, Li Y and Xin L: USP10-dependent stabilization of UGT8 promotes oxaliplatin resistance by sustaining NRF2-associated antioxidant signaling and suppressing ferroptosis in gastric cancer. Free Radic Biol Med 256: 271-284, 2026.
17. Xiao R, Mo Y, Zhou J, Xu Y, Kang K, Chen Z, Jiang Y, Li C, Feng X, Chen Z, *et al*: Inhibition of EphA2 triggers ferroptosis by disrupting USP38mediated SLC7A11 stabilization in chemoresistant gastric cancer. Cell Mol Life Sci 83: 341, 2026.
18. Wu J, Luo D, Tou L, Xu H, Jiang C, Wu D, Que H and Zheng J: NEK2 affects the ferroptosis sensitivity of gastric cancer cells by regulating the expression of HMOX1 through Keap1/Nrf2. Mol Cell Biochem 480: 425-437, 2024.
19. Xue X, Wang M, Cui J, Yang M, Ma L, Kang R, Tang D and Wang J: Glutathione metabolism in ferroptosis and cancer therapy. Cancer Lett 621: 217697, 2025.
20. Zhang M, Zheng H, Zhu X, Liu S, Jin H, Chen Y, Wan L, Zhang S and Zhang H: Synchronously evoking disulfidptosis and ferroptosis via systematical glucose deprivation targeting SLC7A11/GSH/GPX4 antioxidant axis. ACS Nano 19: 14233-14248, 2025.
21. Zhong S, Wang Z, Yang J, Jiang D and Wang K: Ferroptosis-related oxaliplatin resistance in multiple cancers: Potential roles and therapeutic implications. Heliyon 10: e37613, 2024.
22. Li Y, Yang W, Zheng Y, Dai W, Ji J, Wu L, Cheng Z, Zhang J, Li J, Xu X, *et al*: Targeting fatty acid synthase modulates sensitivity of hepatocellular carcinoma to sorafenib via ferroptosis. J Exp Clin Cancer Res 42: 6, 2023.
23. Zhang T, Cao Z, Gao K, Yao S, Zheng Y, Cui M, Yin R, Han G, Hu J, Wang C and Zhang H: PIEZO1 is required for acute myeloid leukemia progression and leukemia stem cell maintenance via HIF1A-SLC7A11 axis-mediated ferroptosis defense. Adv Sci (Weinh) 13: e75648, 2026.
24. Feng Z, Zhang S, Han Q, Chu T, Wang H, Yu L, Zhang W, Liu J, Liang W, Xue J, *et al*: Liensinine sensitizes colorectal cancer cells to oxaliplatin by targeting HIF-1α to inhibit autophagy. Phytomedicine 129: 155647, 2024.
25. Schmittgen TD and Livak KJ: Analyzing real-time PCR data by the comparative C(T) method. Nat Protoc 3: 1101-1108, 2008.
26. Livak KJ and Schmittgen TD: Analysis of relative gene expression data using real-time quantitative PCR and the 2(-Delta Delta C(T)) method. Methods 25: 402-408, 2001.
27. Siddiqui YM, Shakeel I, Hasan GM and Hassan MI: NIMA-related kinase 2: A master regulator of mitotic fidelity and chromosomal instability in cancer: From mechanisms to therapeutic targeting. Biochim Biophys Acta Rev Cancer 1881: 189523, 2025.
28. Xu T, Zeng Y, Shi L, Yang Q, Chen Y, Wu G, Li G and Xu S: Targeting NEK2 impairs oncogenesis and radioresistance via inhibiting the Wnt1/β-catenin signaling pathway in cervical cancer. J Exp Clin Cancer Res 39: 183, 2020.
29. Chen X, Wang C, Yang P, Shi L and Wang H: Ube2s-stabilized β-catenin protects against myocardial ischemia/reperfusion injury by activating HIF-1α signaling. Aging (Albany NY) 12: 5716-5732, 2020.
30. Cao D, Qu Y, Liu J, Wang J, Wei C, Zhou X, Feng J, Ma J, Mur LAJ, Chen L, *et al*: Pteris wallichiana bioactives induce ferroptosis via the SLC7A11-GSH-GPX4 axis to directly suppress colorectal cancer. Phytomedicine 148: 157463, 2025.
31. Ouyang Y, Li Y, Huang Y, Li X, Zhu Y, Long Y, Wang Y, Guo X and Gong K: CircRNA circPDSS1 promotes the gastric cancer progression by sponging miR-186-5p and modulating NEK2. J Cell Physiol 234: 10458-10469, 2018.
32. Chen L, Lu H, Ballout F, El-Rifai W, Chen Z, Gokulan RC, McDonald OG and Peng D: Targeting NEK kinases in gastrointestinal cancers: insights into gene expression, function, and inhibitors. Int J Mol Sci 26: 1992, 2025.
33. Huang X, Zhang G, Tang T, Gao X and Liang T: One shoot, three birds: Targeting NEK2 orchestrates chemoradiotherapy, targeted therapy, and immunotherapy in cancer treatment. Biochim Biophys Acta Rev Cancer 1877: 188696, 2022.
34. Zhao T, Chen X, Wu J, Chen S, Gan Y, Liu C, Ha X, Wu Y, Zhou X, Wu Y and Wu X: YY1-induced USP43 drives ferroptosis suppression by FASN stabilization and subsequent activation of SLC7A11 in ovarian cancer. Cell Death Dis 16: 589, 2025.
35. Zhai D, Xu Y, Ma J, Duangrat R, Yan C, Liang J, Wei H, Jiang B and Li TS: Hydrostatic pressure activates HIF-1α via β-catenin to promote stemness in breast cancer cells. FEBS Open Bio 16: 1992-2002, 2026.
36. Dong S, Liang S, Cheng Z, Zhang X, Luo L, Li L, Zhang W, Li S, Xu Q, Zhong M, *et al*: ROS/PI3K/Akt and Wnt/β-catenin signalings activate HIF-1α-induced metabolic reprogramming to impart 5-fluorouracil resistance in colorectal cancer. J Exp Clin Cancer Res 41: 15, 2022.
37. Zhang H, Pan J, Huang S, Chen X, Chang ACY, Wang C, Zhang J and Zhang H: Hydrogen sulfide protects cardiomyocytes from doxorubicin-induced ferroptosis through the SLC7A11/GSH/GPx4 pathway by Keap1 S-sulfhydration and Nrf2 activation. Redox Biol 70: 103066, 2024.
38. Zhang M, Zheng H, Jin H, Zhu X, Liu S, Chen Y, Zhang H and Zhang S: Regulating SLC7A11/GSH/GPX4 axis by glucose dyshomeostasis to simultaneously promote disulfidptosis, cuproptosis and ferroptosis. Bioact Mater 54: 744-758, 2025.
39. Huang C, Zeng Q, Chen J, Wen Q, Jin W, Dai X, Ruan R, Zhong H, Xia Y, Wu Z, *et al*: TMEM160 inhibits KEAP1 to suppress ferroptosis and induce chemoresistance in gastric cancer. Cell Death Dis 16: 287, 2025.
40. Zhao Y, Liu W, Deng K, Chen Y, Zhou P, Liu C, Jiang G, Wu J, Zhang Y, Qu H, *et al*: LncRNA BASP1-AS1 drives PCBP2 K115 lactylation to suppress ferroptosis and confer oxaliplatin resistance in gastric cancer. Free Radic Biol Med 240: 717-734, 2025.

Copyright © 2026 Tou et al. This work is licensed under a Creative Commons Attribution-NonCommercial-NoDerivatives 4.0 International (CC BY-NC-ND 4.0) License.